Available online at www.sciencedirect.com
ScienceDirect
Polymer 49 (2008) 507–524
polymer
www.elsevier.com/locate/polymer

Gas transport in poly(*n*-alkyl acrylate)/poly(*m*-alkyl acrylate) blends

B.S. Kirkland, D.R. Paul*

Department of Chemical Engineering, Texas Materials Institute, The University of Texas at Austin, Austin, TX 78712, USA

Received 5 September 2007; received in revised form 27 November 2007; accepted 2 December 2007
Available online 5 December 2007

Abstract

Poly(*n*-alkyl acrylate)s can have side chains that crystallize independently of the main chain; side-chain length can thus be used as a tunable parameter to control the gas permeability of membranes. The gas permeation response of poly(*n*-alkyl acrylate) and poly(*m*-alkyl acrylate) blends as a function of temperature is reported for varying side-chain lengths, *n* and *m*, and blend composition in the semi-crystalline and molten states. Macroscopic homogeneity is observed for a small range of *n* and *m* where $|n-m| \leq 2-4$ methylene units. Thermal analysis indicates that the blend components crystallize independently of one another; however, crystallization is hindered by the presence of the other component. Permeation responses of the blends investigated in some cases exhibited two distinct permeation jumps or increases at the melting temperature of each component. Blends with continuous permeation responses but higher effective activation energies of permeation (i.e., more thermally responsive) were observed for some blends over the temperature of interest for membranes to be used for modified atmosphere packaging.

Keywords: *n*-Alkyl acrylates; Gas permeation; Polymer blends

1. Introduction

Polymers with *n*-alkyl pendant side chains have been extensively studied because of their unique properties [1–8]. Poly(*n*-alkyl acrylate)s and poly(*n*-alkyl methacrylate)s have been of particular interest for a variety of applications. When the *n*-alkyl pendant group is sufficiently long, the side chains crystallize independently of the polymer main backbone. The properties of such materials, e.g., flow behavior, adhesion, and permeability to small molecule penetrants, can change dramatically as the melting point of side-chain crystals is traversed [9–11]. Thus, side-chain crystallinity can be a useful design parameter controlled by the side-chain length.

The concept of thermally tunable properties has made poly(*n*-alkyl acrylate)s attractive for many applications, from pressure sensitive adhesives [12] for medical applications to smart membranes [13] for modified atmospheric packaging. Modified atmospheric packaging (MAP) technology utilizes polymeric membranes to regulate the O_2 entering and the CO_2 leaving from a package containing fruits or vegetables to extend shelf life. However, it has proved challenging to design membranes with appropriate transmission rates to safely package continually respiring produce when the storage temperature varies since produce respiration rates vary more strongly with temperature than do permeation rates [14]. Side-chain crystalline polymers may offer an avenue for making membranes that are more thermally responsive for MAP by taking advantage of the dramatic increase in permeability as the melting point of the crystallites is traversed. The idea is to spread this change over a broader range of temperatures.

The gas permeability of random copolymers of *n*-alkyl acrylate monomers of varying side-chain length was examined in recent reports from this laboratory [15,16]. Similar to poly(*n*-alkyl acrylate) homopolymers, these random copolymers exhibit a single permeability jump. The purpose of this paper is to explore the gas transport properties of poly(*n*-alkyl acrylate) homopolymer blends and to contrast their behavior with corresponding copolymers.

* Corresponding author. Tel.: +1 512 471 5392; fax: +1 512 471 0542.
E-mail address: drp@che.utexas.edu (D.R. Paul).

0032-3861/$ - see front matter © 2007 Elsevier Ltd. All rights reserved.
doi:10.1016/j.polymer.2007.12.002

2. Background

2.1. Properties of poly(n-alkyl acrylate)s

Side-chain length has a profound effect on the physical, thermal and transport properties of poly(*n*-alkyl acrylates); side-chain crystallization is possible when there are approximately 9–10 carbon atoms extending beyond the ester group connection to the main chain, but below this critical side-chain length no crystallization occurs. Jordan and others [17] observed a linear increase in the heat of fusion with side-chain length, *n*. The first 9–10 carbon atoms of the alkyl side chain closest to the backbone reside in the amorphous phase while the remaining alkyl side chain crystallizes into a layered configuration with alternating amorphous and crystalline phases. Upon crystallization, the side chains of poly(*n*-alkyl acrylate)s crystallize into a hexagonal crystal structure as characterized by wide angle X-ray studies in conjunction with the presence of a single IR adsorption band in the 720 cm^{-1} region [18–20]. It is generally accepted that side chains crystallize into a one-layer arrangement, where side chains pack end-to-end, or a two-layer arrangement, where side chains pack in an interdigitating manner as proposed by Platé [19,21]. Both arrangements, dependent on crystallization conditions, have been observed for the side chains of poly(*n*-alkyl acrylate)s, but the single layer is more dominative attributable to the flexible backbone allowing more uniform and efficient packing compared to other side-chain crystalline polymers. As the side-chain length increases, the crystallites become thicker increasing the heat of fusion and the melting temperature and thereby altering the polymer performance.

2.2. Gas transport in semi-crystalline polymers

Small molecule gas permeation through dense or nonporous polymer films occurs by a solution-diffusion mechanism. Gas molecules are sorbed into the upstream polymer surface at high pressure, diffuse through the film and then desorb downstream on the low pressure side. The gas permeability coefficient

$$\boldsymbol{P} = DS \tag{1}$$

is the product of *D*, the gas diffusion coefficient and *S*, the solubility coefficient [22]. The diffusion coefficient is a kinetic parameter that reflects the mobility of the penetrant in the polymer matrix and the solubility coefficient is a thermodynamic parameter that depends on the polymer–penetrant interactions as well as penetrant condensability. Sorption of simple gases through rubbery polymers at moderate pressures is well-described by Henry's law

$$C = Sp \tag{2}$$

where *C*, the penetrant equilibrium concentration, is proportional to *p*, its partial pressure, and *S*, the solubility coefficient of the gas in the polymer. In the case of semi-crystalline poly(*n*-alkyl acrylates), gas transport is more complex than in simple amorphous polymers owing to side-chain crystallinity. Michaels et al. introduced a two-phase model that modified the solubility and diffusion coefficients to account for the presence of crystallites in semi-crystalline polyethylene. Experimental results suggest that the solubility in several polyethylenes of varying crystallinity is proportional to the amorphous volume fraction, α

$$S = S^*\alpha \tag{3}$$

where S^* is the solubility coefficient in a completely amorphous polymer sample [23]. These results imply that the crystals are impenetrable to gas permeation. The crystals affect the diffusion coefficient in two separate ways as described by the following [24]:

$$D = D^*/\tau\beta \tag{4}$$

where D^* is the penetrant diffusion coefficient in the amorphous phase, τ is a geometric impedance factor, and β is a chain immobilization factor. The geometric impedance factor accounts for the tortuous path the gas molecules must take through the amorphous phase since they cannot permeate through the crystallites. The chain immobilization factor accounts for reduced mobility of the amorphous phase caused by the crystallites. Finally, the permeability coefficient can be expressed as follows:

$$\boldsymbol{P} = P^*\alpha/\tau\beta \tag{5}$$

where P^* is the permeability of a completely amorphous sample. The thermal history of a polymer can significantly affect crystallite size, shape, and orientation and, in turn, affect permeation properties.

The temperature dependence of the gas permeability coefficient is generally described by an Arrhenius relationship:

$$\boldsymbol{P} = P_o e^{-E_p/RT} \tag{6}$$

where E_p is the activation energy and P_o a constant. If α, β and τ are all constant, then the activation energy for gas permeation in the semi-crystalline state should be the same as in the molten state; however, this is generally not the case [25], and this is usually attributed to the temperature dependence of β when the crystalline content and morphology are fixed [25]. However, in some cases, melting can occur progressively over a range of temperatures such that α and τ are changing, and this will increase the effective activation energy for permeation which can be useful for making membranes that are more thermally responsive as needed for some packaging applications.

2.3. Permeability in poly(n-alkyl acrylate)s and their utility as thermally responsive membranes

Mogri and Paul [25] found that gas permeability increases, for *n*-alkyl acrylate homopolymers, as a function of side-chain length for completely amorphous polymers ($n < 10$ or $T > T_m$) due to increased free volume. Below the melting point of

poly(*n*-alkyl acrylates) that crystallize, the permeability is greatly reduced owing to the tortuous path the gas molecules must follow within the amorphous phases since the crystallites are impenetrable and the constraints these crystallites impose on molecular motions within the amorphous phase [23,24]. There is a jump in the gas permeability by a factor of 10–100 upon traversing the melting point that is primarily diffusion based [9]. A similar jump is observed for copolymers of *n*-alkyl acrylate monomers since they show a single melting point following the rules of co-crystallization or melting point depression depending on the side-chain length [15,16].

The increase in permeability that results from melting the side-chain crystals provides an interesting avenue to create membranes that are more thermally responsive than can be achieved by the usual Arrhenius response. One approach would be to create laminates composed of successive layers of poly(*n*-alkyl acrylate) of varying side-chain length as suggested in Fig. 1. Each layer, *i*, has a different melting point with a corresponding permeability jump. The composite permeability coefficient can ideally be described by a series models:

$$\frac{l}{\boldsymbol{P}} = \sum_{i=1}^{N} \frac{l_i}{\boldsymbol{P}_i} \tag{7}$$

where l_i is the thickness of polymer *i* and $\boldsymbol{P}_i$ is the permeability of polymer *i* [22]. In principle, as more layers are added, the more closely the successive step functions approach a monotonic function like the dotted line shown. This would be facilitated by broadening the crystallite distribution and allowing crystallites to melt over a wider range of temperatures thereby increasing the breadth of the permeability jump. An interesting alternative to the highly structured laminates of Fig. 1 is to make blends of two or more homopolymers or copolymers of *n*-alkyl acrylate monomers of varying *n*. The basic issues associated with this strategy are explored here.

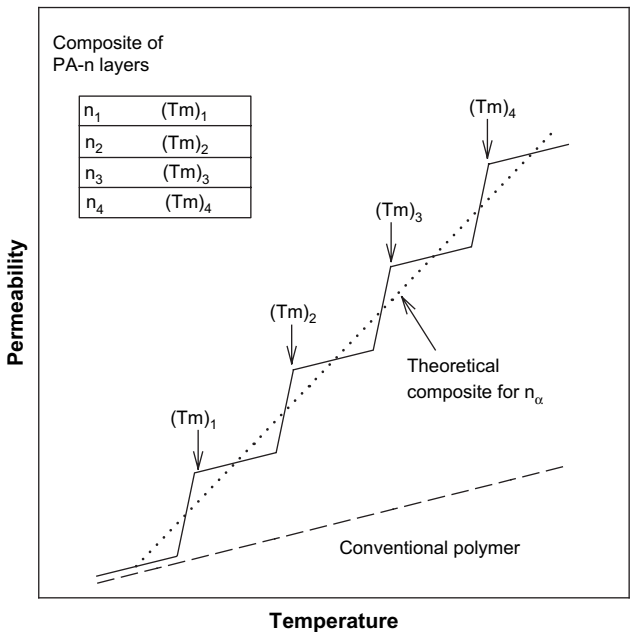

Fig. 1. Illustration of the use of laminates with multiple layers of poly(*n*-alkyl acrylate)s with varying side-chain length, *n*, to increase the thermal response of gas permeation.

3. Materials, blend formation and characterization methods

Hexyl (A-6), octyl (A-8), and decyl (A-10) acrylate monomers were purchased from Scientific Polymer Products. Tetradecyl (A-14), hexadecyl (A-16), octadecyl (A-18) and behenyl (A-22) acrylate monomers were donated by Landec Corporation. All monomers were dissolved in toluene and purified over Sigma–Aldrich aluminum oxide to remove a low concentration inhibitor, monomethyl ether hydroquinone (MEHQ). Amorphous monomers at room temperature are mixed directly with solvent; however, A-18 and A-22 monomers were more carefully handled as they tend to crystallize and stratify. Whatman® 0.2 μm filter membrane discs were used to filter out particulate impurities from the monomers; following this, the monomers were ready for polymerization. Free radical solution polymerization was performed using 35 wt% monomer in toluene at 60 °C for 24 h to achieve nearly 100% conversion of atactic polymer [26]. Solutions were charged into a three-neck round bottom flask and purged with N_2 to remove oxygen (possible inhibitor) and subsequently charged with purified initiator, α,α′-azobis(isobutyronitrile) (AIBN) [27]. After 24 h, the polymer product was slowly precipitated into ethanol, recovered and purified by using toluene/ethanol re-precipitation through three cycles. The polymers were characterized by gel permeation chromatography (GPC), calibrated using polystyrene standards, to determine relative molecular weights. A Perkin–Elmer DSC-7 differential scanning calorimeter, equipped with an intercooler capable of measurement from −40 °C, was used to determine the melting points and heat of fusion. The DSC-7 was calibrated with certified reference materials, indium and zinc. However, the semi-crystalline materials analyzed had comparatively low melting points; therefore, 4-nitrotoluene was also used as a calibration standard. All samples were subjected to a series of heating and cooling cycles to eliminate the influence of previous thermal history, thus, to ensure identical crystallization conditions for comparative morphologies. Therefore, all thermal properties were analyzed on second heating cycles from a 1 °C/min cooling rate with subsequent heating at 10 °C/min to ensure a common thermal history.

All homopolymer and polymer blend films were formed by solution casting techniques with the exception of PA-8, PA-10 and PA-14. The latter are all soft, tacky, amorphous polymers at room temperature; therefore, they were cast directly onto a custom composite support [28] in an enclosed oven at elevated temperatures. Samples were allowed to equilibrate forming a smooth, uniform film. Sample thickness was calculated by mass balance techniques using an estimated amorphous density of 0.985 g/cm^3. All other polymer systems were solid, brittle materials at room temperature. This brittleness stems from the side-chain crystalline character and is not owing to low sample molecular weight [1,29]. These polymer systems were solution

cast from 5–10 wt% polymer in toluene onto silicon wafers and covered for slow evaporation in a fume hood. Films formed in this way were subsequently removed by using water to release them from the silicon surface and placed under vacuum at elevated temperatures for further solvent removal. Depending on the melting temperature of the polymers involved, removal from the casting surface could require using cool water and subsequent cool storage. PA-8/PA-10 blends were formed by this same method and then cast directly onto the custom composite support similar to the above mentioned amorphous samples [30]. For polymers that were solid at room temperature, the polymer thickness was measured using a micrometer before assembling the composite.

For gas permeability measurements of poly(*n*-alkyl acrylate) films, a modified sample assembly was developed in our laboratory [28] that supported their brittle nature below the melting point and liquid-like behavior above T_m. An asymmetric Whatman Anopore™ porous ceramic disc without the annular polypropylene support ring was used for mechanical support. The ceramic discs have 200 Å pores on the surface that extend to ~1 μm below the surface and connect to 2000 Å pores. Permeability measurements above the melting point required a suitable polymer coating to prevent molten polymer from flowing into the ceramic disc pores and changing the apparent polymer thickness. Poly(2,6-dimethyl-1,4-phenylene oxide) (PPO), from General Electric Plastics with an intrinsic viscosity of 0.46 dL/g, $M_w = 46{,}000$ and a $T_g \sim 220$ °C, was used to coat the top surface of the ceramic disc. A trichloroethylene solution containing 13 wt% PPO was deposited onto the ceramic disc using 2 mL syringes spread by a scoopula which removed excess PPO solution which left a thin film that completely seals the ceramic pores.

Permeability experiments were conducted using constant volume permeation cells, at an upstream pressure of 2 atm [31], immersed in a water-bath equipped with a temperature controlled Haake circulator. Permeability measurements were made with a range of gases, He, H_2, O_2, N_2, CH_4 and CO_2, from Matheson Tri-gas with a minimum 99.9% purity. However, for brevity, we report here only the permeation results of O_2 as a typical example with an occasional comparison to N_2 and CO_2 as these gases are of interest for MAP. The permeation results for other gases may be found elsewhere [30]. Prior to testing the *n*-alkyl acrylate polymers, the quality of the support assembly was determined by comparing gas permeation selectivities with literature values for PPO to ensure that the pores were completely sealed. Upon adequate support selection, the permeance of the thin, glassy PPO layer was characterized to account for physical aging. After quantifying the physical aging response, the poly(*n*-alkyl acrylate) film was placed on top of the assembly for permeability determination. The measured composite permeation resistance was corrected for the contribution of the PPO layer, which was always less than 5% of the total except for CH_4 where it sometimes was as high as 15%, to obtain just the contribution of the poly(*n*-alkyl acrylate) film.

As mentioned previously, thermal history can have a discernable effect on phase morphology and subsequently on permeation properties. Therefore, a Linkman hot-stage, model HFS91, and a programmable controller, model TMS91, system were used to establish a known polymer thermal history. Samples were heated to approximately 10 °C above the polymer melting point and held for sufficient time to completely remove any residual crystallinity and then cooled mostly at a rate of 1.0 °C/min except for a few variable rate experiments.

4. Results and discussion

4.1. Poly(n-alkyl acrylate) blend compatibility

A fundamental issue is whether blends of a poly(*n*-alkyl acrylate) and a poly(*m*-alkyl acrylate) are miscible in the molten state, and if so, do they co-crystallize on cooling. Clearly, both issues may be influenced by the values of *m* and *n*; the closer *m* and *n* are to each other, the more likely the two polymers are to be miscible and exhibit co-crystallization. At a practical level, the question is over what ranges of *m* and *n* can useful membranes be cast by the procedures used here. To explore this, 50/50 weight blends were prepared by solution casting films of all combinations of poly(*n*-alkyl acrylate) homopolymers with side-chain lengths, *m* and *n*, from 6 to 22. Each binary homopolymer blend was inspected visually for homogeneity. Fig. 2 shows a matrix of the results of this simple assessment where the coordinates represent the homopolymer components of a binary blend by the lengths of their side chains, *n* and *m*. The solid line represents the limiting case of blends with the same side-chain length which, of course, are homogenous. Viable homogeneous blends are represented by the filled circles. These blends were optically clear in the melt and macroscopically homogenous after crystallization.

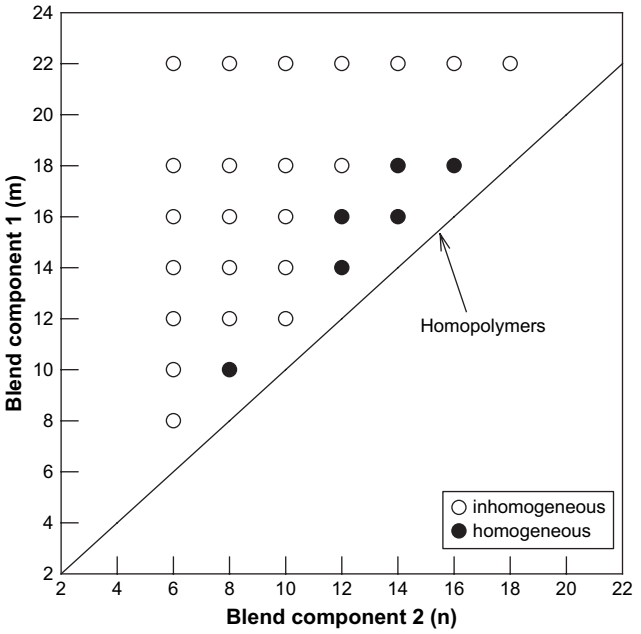

Fig. 2. Map of film homogeneity for 50/50 weight poly(*m*-alkyl acrylate) and poly(*n*-alkyl acrylate) blends with side-chain lengths, *m* and *n*; the filled circles represent homogeneous mixtures while the open circles represent grossly heterogeneous mixtures.

PA-8 and PA-10, the only feasible amorphous blends, were clear at room temperature and for the temperature range of interest. Semi-crystalline blends were transparent above the melting point and by nature opaque at room temperature with varying degree of clarity depending on m and n. Inhomogeneous blends are indicated by open circles. Although all inhomogeneous blends appeared optically clear in the amorphous and melt states, upon cooling or crystallization two phases were easily distinguishable. Heterogeneous blends containing two amorphous components resulted in a transparent mixture with two separate phases noticeable only by slight density differences. Inhomogeneous systems with one amorphous and one semi-crystalline components and with two semi-crystalline component mixtures resulted in varying heterogeneous morphologies influenced by the blend components (n and m) and composition. For the most part, the components of inhomogeneous blends exhibited macroscopic segregation. Thermal analyses conducted on samples from various regions within a given polymer–polymer mixture resulted in widely varying thermal properties indicating gross phase segregation using this film preparation technique. In general, homogeneity was observed when the difference in side-chain length ($n - m$) between components was small, $|n - m| \leq 2$–4 methylene units, and when the components possessed similar crystallization characteristics. Surprisingly, neither PA-10 nor PA-22 resulted in any homogenous semi-crystalline blends regardless of the choice of the other component.

It would be useful to know over what range of m and n these blends are miscible in the melt state; however, such a determination is a very challenging experimental problem. Blend miscibility is often assessed by determining glass transition temperature (T_g) behavior. However, the glass transitions of poly(n-alkyl acrylates) occur at very low temperatures and are difficult to measure with any accuracy and reliability owing to the side-chain crystallinity. It was well beyond the scope of this work to pursue the issue of miscibility further.

4.2. Thermal characterization

Thermal characterization has proved to be a useful tool for predicting the permeation response of n-alkyl acrylate polymers as a function of temperature [15,16,25]. Table 1 summarizes the melting temperature, heat of fusion, crystallinity and molecular weight of the semi-crystalline ($n \geq 10$) n-alkyl acrylate homopolymers, with thermal histories, used in this study. The melting point and the heat of fusion, ΔH_f, or crystallinity, x_c, increase as the side-chain length increases [25].

Fig. 3 shows DSC thermograms for blends of PA-14 and PA-18 which are typical of all the blends of semi-crystalline poly(n-alkyl acrylate) and poly(m-alkyl acrylate) blends examined. For the pure components, the peak width decreases as side-chain length increases suggesting a narrowing of the crystallite distribution [32]. The blends show two endothermic peaks implying independent crystallization of the respective components (i.e., no co-crystallization). The magnitude of the component peaks became larger as the content of that component in the blend increases as expected. The melting point for each component, taken as the apex of the peak, shifts to a slightly lower temperature upon dilution by the other polymer, as shown in Fig. 4, suggesting some alteration of the crystal formation due to blending;

Table 1
Thermal and physical properties of semi-crystalline polymers studied in this work

Polymer	T_m (°C)	ΔH_f (cal/g)	x_c	M_w
PA-14	22.4	16.6	0.32	307,000
PA-16	36.2	19.5	0.37	204,000
PA-18	50.2	22.9	0.44	175,000

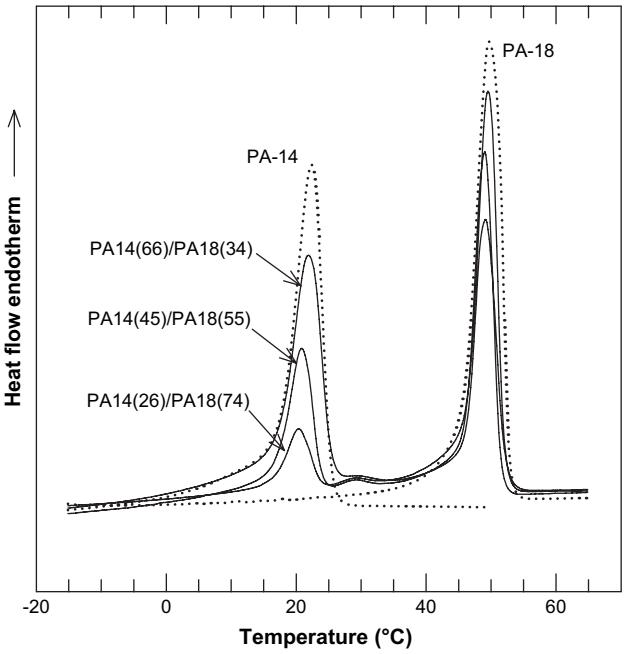

Fig. 3. DSC scans for PA-14/PA-18 blends of various compositions.

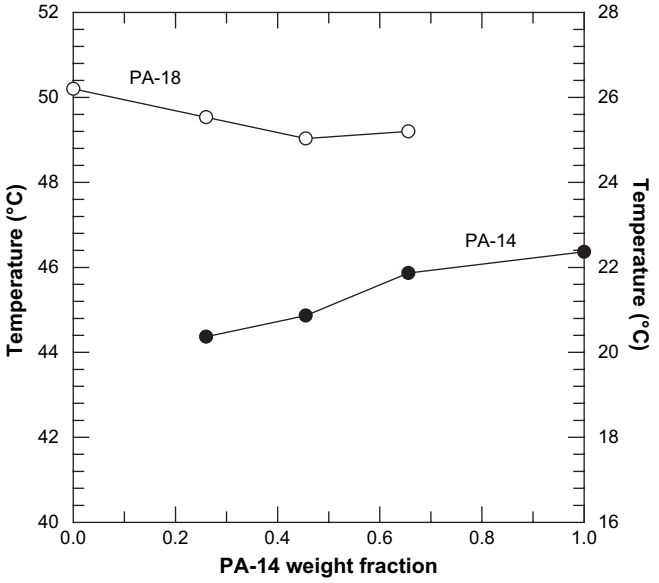

Fig. 4. Melting temperatures of the components in PA-14/PA-18 blends as a function of blend composition.

however, the effect is very small with the maximum shift in T_m being of the order of 2 °C. Extracting heat of fusion for each component from the thermograms requires some assumptions about how to construct the baseline and interpret of some subtle features of the DSC traces. A small but distinguished third peak can be seen between the peaks of the two blend components; this intermediate peak could be a result of co-crystallization or simply overlap from the individual melting transitions. This peak is visible at various scanning rates suggesting that it is not an artifact.

A straight [33] baseline construction was used in the two methods of interpretation described next. In the first method, a nearly horizontal, straight baseline was drawn from the initial point of deviation to the point where the signal returned to the baseline, enclosing the entire area under the PA-14, PA-18 and the intermediate peaks as illustrated in Fig. 5(a). The area defined in this way is considered to be the total heat of fusion for the blend, ΔH_{blend}. In the second method, separate baselines are constructed for each major peak. The area under the first peak is designated as the heat of fusion for the low melting component or ΔH_1. Similarly, the area under the second peak is designated as the heat of fusion for the higher melting component or ΔH_2. The sum of the individual heat of fusion for each component, $\Delta H_{sum} = \Delta H_1 + \Delta H_2$, could also be interpreted as the total heat of fusion for the blend components. Fig. 5(b–d) show the heat of fusion values calculated by each of these methods, ΔH_{blend} represented by filled circles and ΔH_{sum} by open circles. If the individual components in the blend crystallize without any interference from the other blend component, then one would expect heat of fusion for the individual components or the total heat of fusion for the blend as a function of blend composition to form straight lines connecting the end points at the two composition extremes represented as dashed lines in Fig. 5(b–d). The values calculated by the baseline construction methods described above always fall below these additivity relations. The values of ΔH_{blend} come closer to this ideal than the attempts to separate the melting processes of the two components. In general, it seems

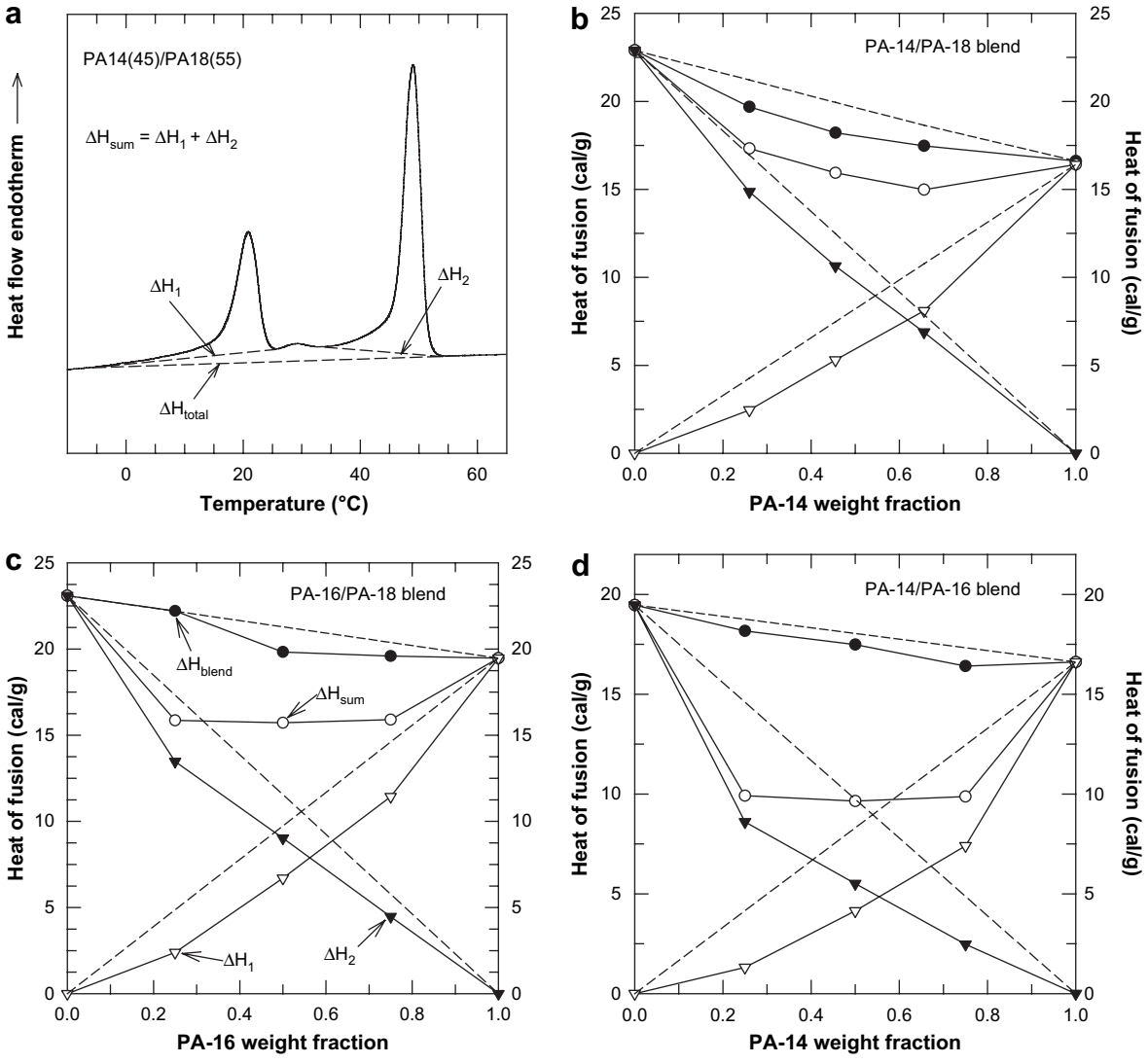

Fig. 5. (a) Illustration of baseline construction methods used to compute heat of fusion from blend thermograms. Heat of fusion as a function of composition for (b) PA-14/PA-18 blends, (c) PA-16/PA-18 blends, and (d) PA-14/PA-16 blends.

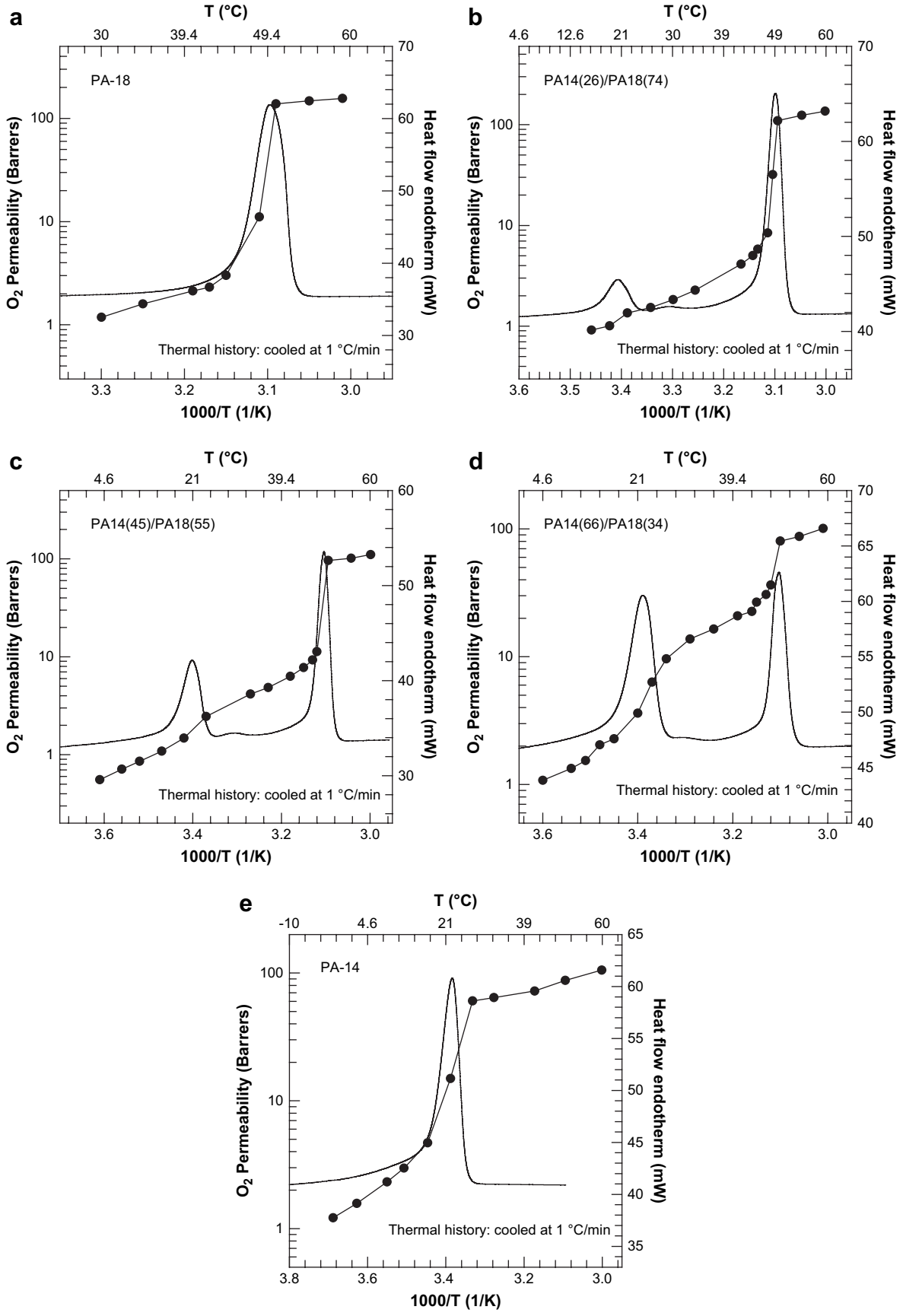

Fig. 6. O_2 permeability and DSC thermograms for (a) PA-18 homopolymer, (b) PA-14(26 wt%)/PA-18(74 wt%) blend, (c) PA-14(45 wt%)/PA-18(55 wt%) blend, (d) PA-14(66 wt%)/PA-18(34 wt%) blend, and (e) PA-14 homopolymer.

clear for these blends that one component has some effect on the crystallization and, hence, melting behavior of the other. Owing to the difficulties associated with knowing the correct baseline construction, it is not possible to be more precise about these effects. Certainly if any degree of co-crystallization occurs, it is very slight indeed.

4.3. Permeation behavior

4.3.1. Poly(tetradecyl acrylate) and poly(octadecyl acrylate) blends

Fig. 6 shows the permeation behavior of PA-14 and PA-18 blends with their corresponding DSC thermograms. As mentioned in the previous section, polymer films were cooled at a fixed rate of 1.0 °C/min to provide similar thermal histories since permeability depends on the resulting crystalline morphology which is controlled by the thermal history. A subsequent section briefly addresses the effect of cooling rate on the permeability of poly(*n*-alkyl acrylate) blends. Permeability switch behavior of the homopolymers shown in Fig. 6(a,e) is similar to what has been reported previously [25]. The permeability varies linearly with temperature above and below the melting temperature of the side-chain crystallites with differing slopes (i.e., activation energies for permeation). As the melting point is traversed, there is a dramatic increase in permeability. As the side-chain length decreases, the breadth of the permeation switch increases as a result of a broader crystallite distribution. As shown in Fig. 6(b–d), PA-14 and PA-18 blends exhibit two distinct permeation jumps that occur at the melting point of each independently crystallized component, thus spreading the overall permeation jump over a wider temperature range. There is an intermediate state between the melting points of the pure polymers where the permeability again increases linearly, on these coordinates, with temperature. The slight shift of melting points on blending was not observable for the permeation jumps; this is more clearly seen in Fig. 7 where permeation responses for PA-14/PA-18 blends in the full compositional range are shown in one plot. It is also evident that the magnitude of the permeation jump for each polymer component increases as the amount of the respective component increases in the blend. At high concentrations of the shorter side-chain length chain component, it is apparent that its permeation switch is effectively reduced due to hindered crystallization resulting from the presence of the other polymer; this is supported by the lower than additive crystallinity or heat of fusion shown in Fig. 5(b). Although only O_2 gas permeability is shown here, other gases showed analogous responses, but with some quantitative differences; the magnitude of the permeation jump has been shown to be dependent on penetrant size [9]. There is a commensurate increase in the magnitude of permeation jump as the quantity of the respective component increases, and this response is not strictly linear. By quantifying the magnitude of the permeation switch, we can see this more explicitly.

A convenient method to quantify the homopolymer permeation switch was previously established [34]. The existence of two types of crystallites required modification of this method

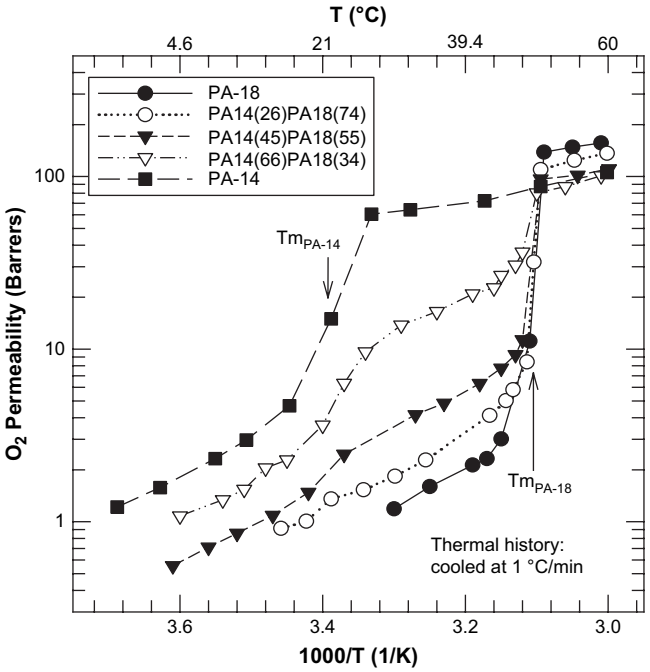

Fig. 7. Comparison of O_2 permeabilities for various PA-14/PA-18 blends as a function of temperature.

in order to quantify the two permeation jumps observed for crystalline *n*-alkyl acrylate polymer blends; this modified method is illustrated in Fig. 8. The permeation jump is conveniently represented as the ratio of the penetrant permeability

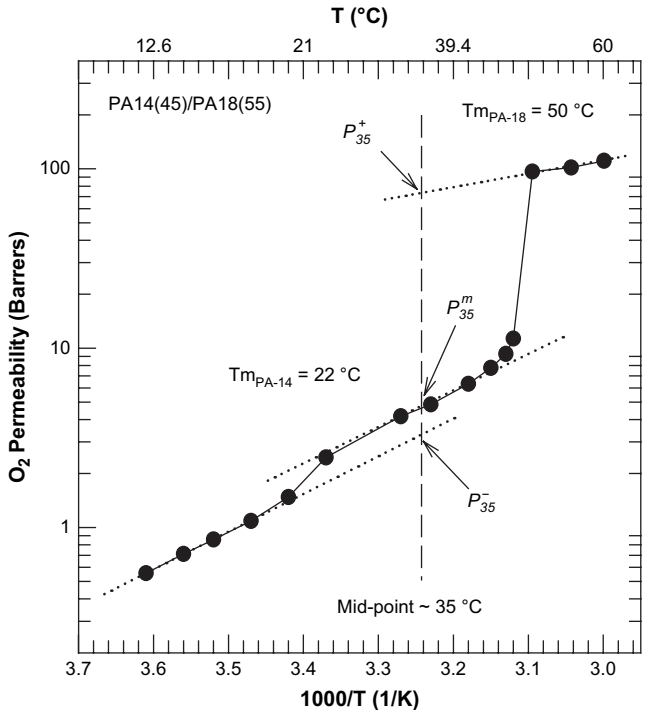

Fig. 8. Illustration of the procedure used to calculate the magnitude of the permeation jumps for an arbitrary reference temperature of 35 °C. The permeability in the semi-crystalline state, P^{-}_{35}, in the intermediate state, P^{m}_{35}, and in the molten state, P^{+}_{35}, were evaluated at or extrapolated to 35 °C.

coefficient in the molten state to that in the semi-crystalline state at temperature T. The magnitude of the jump can vary significantly depending on the temperature chosen due to the difference in activation energies for permeation above and below the melting temperature [25]. In evaluating the blends, we have chosen to use a temperature, T, midway between the melting points of the two pure polymers; in the case shown, T is 35 °C. Below the melting temperatures of both components, the solid-state permeability is determined by extrapolation to the mid-point temperature and is designated as $\boldsymbol{P}_T^-$ where the superscript minus sign denotes the solid state. It is important to obtain a representative baseline for meaningful extrapolation of permeability values by starting well below the melting point of the low-temperature component. In some cases, the more brittle nature of the higher melting components in the blend prevented permeation measurements at low temperatures necessary for good baseline determination. Above the melting point of the low melting component but below the melting point of the other component, there exists an intermediate state where the only crystallites are from the higher melting component. The permeability coefficient in this intermediate state is designated as $\boldsymbol{P}_T^{\mathrm{m}}$ where the superscript letter "m" denotes the intermediate state. Above the melting point of the high-temperature melting component, the molten state permeability coefficient is designated as $\boldsymbol{P}_T^+$. For the case considered, the ratios of these parameters are used to measure the magnitude of the permeation jumps for the low-temperature component PA-14, $\boldsymbol{P}_{35}^{\mathrm{m}}/\boldsymbol{P}_{35}^-$, the high-temperature melting component PA-18, $\boldsymbol{P}_{35}^+/\boldsymbol{P}_{35}^{\mathrm{m}}$ and the overall permeability jump for the blend, $\boldsymbol{P}_{35}^+/\boldsymbol{P}_{35}^-$.

Fig. 9 shows each of these ratios for the PA-14 and PA-18 blends as a function of blend composition. As evident from the graphs, the permeation switch magnitude is somewhat dependent on gas penetrant size; the permeation switch magnitudes increase from O_2, CO_2 to N_2. Among the gas permeation jumps examined here, nitrogen generally has the

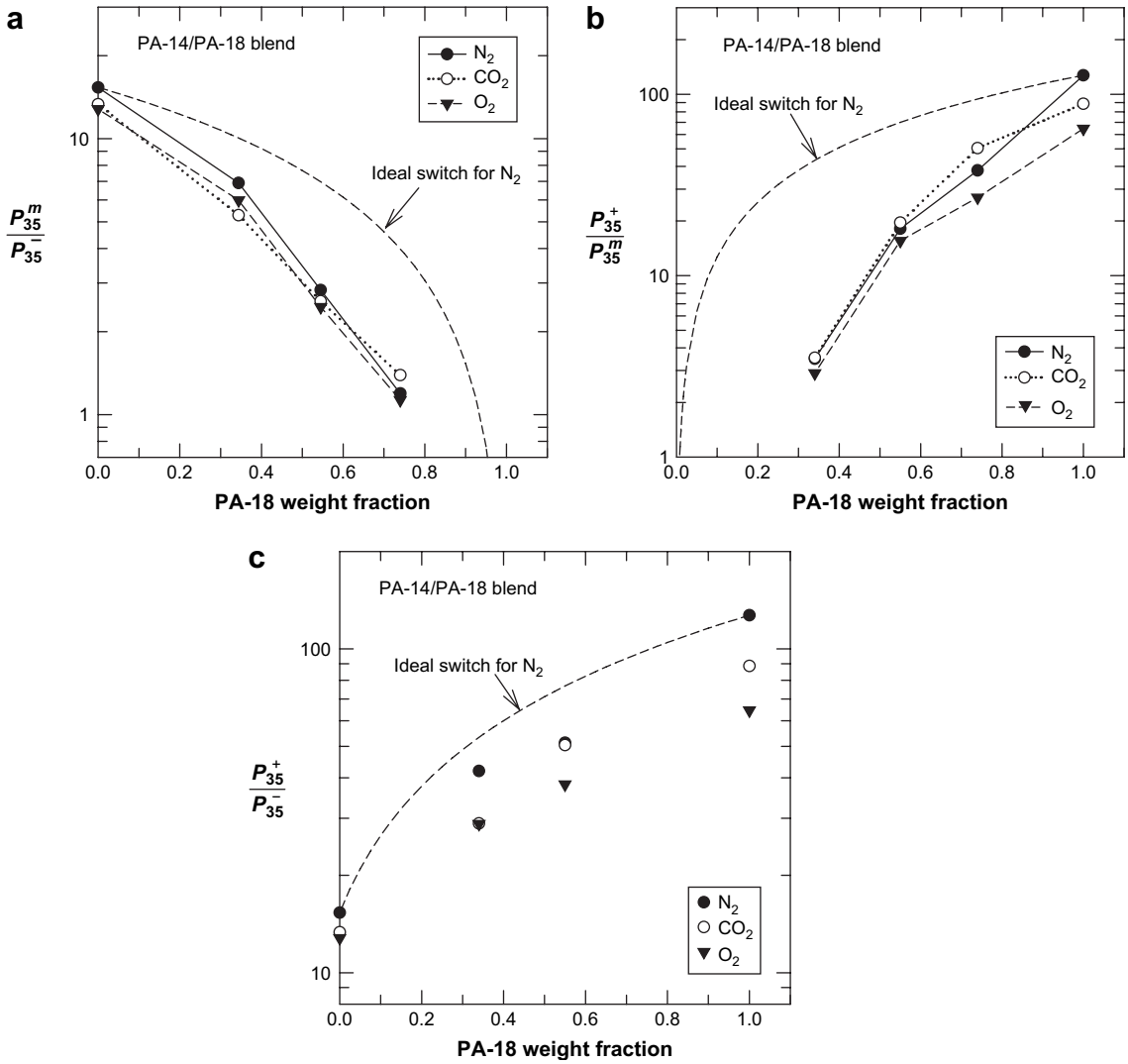

Fig. 9. The magnitude of O_2, N_2, and CO_2 permeation jumps for PA-14/PA-18 blends as a function of composition for (a) the PA-14 blend component, (b) the PA-18 blend component, and (c) the overall blend. Note: the baseline for the PA-14(26 wt%)/PA-18(74 wt%) blends was assumed to be well established when computing the magnitude of the overall permeation jump.

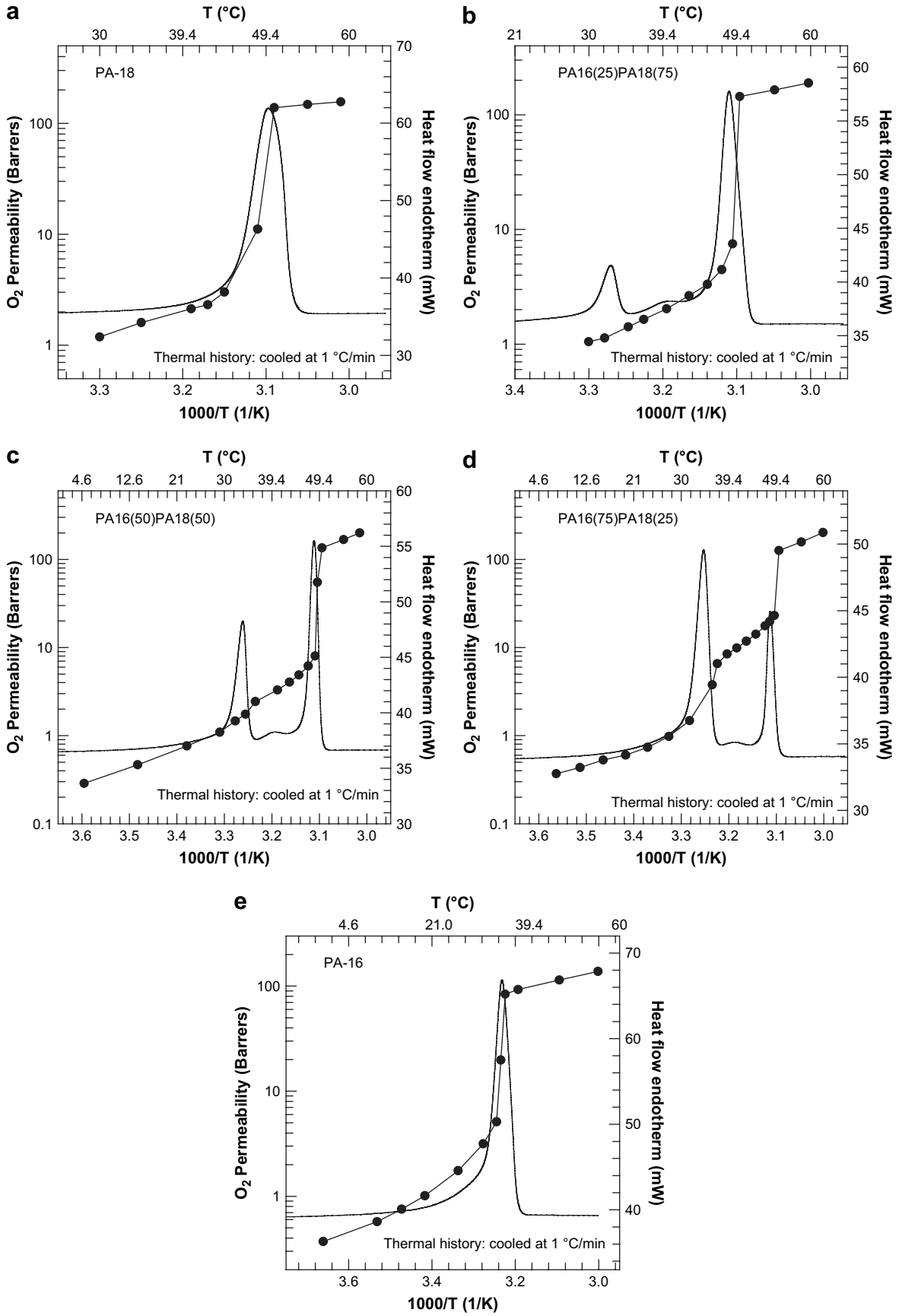

Fig. 10. O_2 permeability and DSC thermograms for (a) PA-18 homopolymer, (b) PA-16(25 wt%)/PA-18(75 wt%) blend, (c) PA-16(50 wt%)/PA-18(50 wt%) blend, (d) PA-16(75 wt%)/PA-18(25 wt%) blend, and (e) PA-16 homopolymer.

largest permeation switch. For comparative purposes, an ideal permeation switch for nitrogen was computed assuming the quantity of a given pure component added to the blend crystallized without any influence from the other component. This ideal N_2 permeation jump for the PA-14 component in the blend is assumed to be represented by the following expression:

$$\left(\frac{P^{m}_{35}}{P^{-}_{35}}\right)_{PA\text{-}14} = w_{PA\text{-}14}\left(\frac{P^{m}_{35}}{P^{-}_{35}}\right)^{o}_{PA\text{-}14} \quad (8)$$

That is, the N_2 jump ratio for PA-14 in the blend is directly proportional to the weight fraction of PA-14 in the blend, $w_{PA\text{-}14}$, times the permeation jump for pure PA-14. The ideal permeation jump for PA-18 is represented by a similar expression. The ideal permeation switch magnitude for each blend component is represented by the dashed lines in Fig. 9(a,b). These lines are not a linear function of blend composition because of the semi-logarithmic coordinates used here. Both permeation jumps for the individual components in the blend lie below this dashed curve for all penetrants indicating the permeation switch is suppressed somewhat by blending. An ideal overall N_2 permeability jump for the blend can be more generally expressed as an additive function:

$$\left(\frac{P^{+}_{T}}{P^{-}_{T}}\right)_{blend} = w_i\left(\frac{P^{m}_{T}}{P^{-}_{T}}\right)^{o}_{i} + w_j\left(\frac{P^{+}_{T}}{P^{m}_{T}}\right)^{o}_{j} \quad (9)$$

where w represents the weight fraction of each component, i is the low-temperature melting component and j being the high-temperature melting component, and the ratios are the respective pure component permeation jumps. The value of this ideal overall N_2 permeation switch for the blend is shown as the dashed curve in Fig. 9(c). The measured blend permeation jump is lower than this additivity curve suggesting again that the permeation jumps are somewhat suppressed in the blend.

The permeation switches for the PA-14/PA-18 blends are always lower than the ideal cases, which is similar to the heat of fusion values which lie below the additivity lines indicating the components do not crystallize as though the other component was not present. The lowered permeation switch effect may reflect smaller, less perfect crystals being formed in the blend.

4.3.2. Poly(hexadecyl acrylate) and poly(octadecyl acrylate) blends

Representative permeation responses for PA-16/PA-18 blends and the pure components are shown in Fig. 10. Similar to PA-14 and PA-18 blends, thermograms show that there are also two endothermic peaks for the blends indicating there is no significant co-crystallization between the components. The size of each peak appears to increase proportionately to the amount of polymer added. Although the T_ms are closer, i.e., 36 and 50 °C, than that for the PA-14/PA-18 blend components, the peaks are still resolvable without significant overlap. Generally, two separate permeation switches are observed for PA-16/PA-18 blends with the exception of the PA-16(25)/PA-18(75) blend. The absence of a permeation jump for the PA-16 component suggests that the melting of small crystals observable by DSC did not cause ample morphological changes to cause a permeation jump or there was insufficient low-temperature data to adequately define the small permeation jump. Comparing the response of the PA-16(25)/PA-18(75) blend to that of PA-14(26)/PA-18(74) in Figs. 10(b) and 6(b) would suggest that the former is true; a minute permeability change is observed at the melting temperature of the shorter side-chain component. Fig. 11 shows that the permeation switch for each blend occurs very close to the melting temperature of the pure components. The difference between the solid-state permeability of these pure components is small, and as a result, the PA-16 and PA-18 blends show negligible changes in the absolute permeability upon blending and its value is closer to that of the longer side-chain length component, PA-18. The heat of fusion for the blend by both methods shows very little change upon blending which support this observation. In the melt, the permeability for this blend system is between that of both components.

Fig. 12 shows the oxygen permeation switch values at 43 °C as a function of PA-16/PA-18 blend composition. The permeability jumps for PA-16 in the blends is lower than the ideal N_2 permeation jump computed for each blend composition. The PA-18 component permeation jump was lower than the ideal curve except for O_2 and N_2 for the 50/50 weight blend which is in agreement with what is expected based on the PA-18 content in the blend. The overall permeation switch for the blend is higher than the ideal dashed curve, but consistent with the solid and molten state trends. The magnitude of

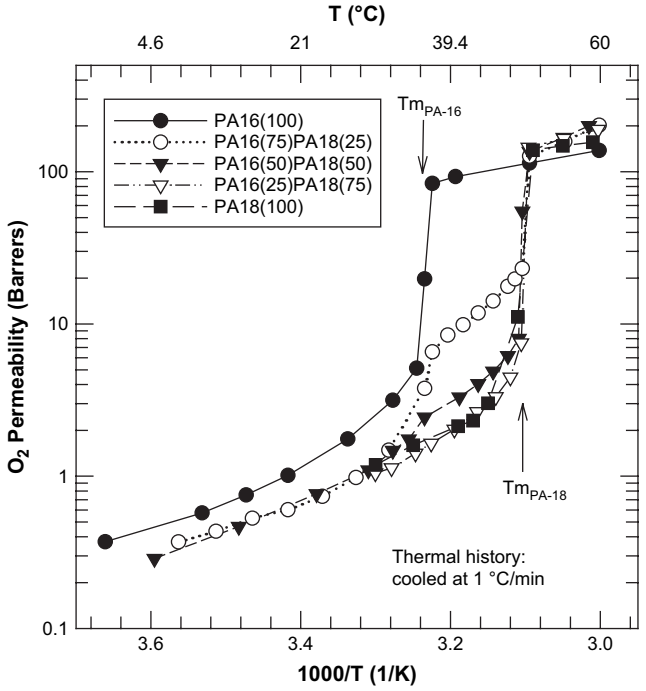

Fig. 11. Comparison of O_2 permeability for various PA-16/PA-18 blends as a function of temperature.

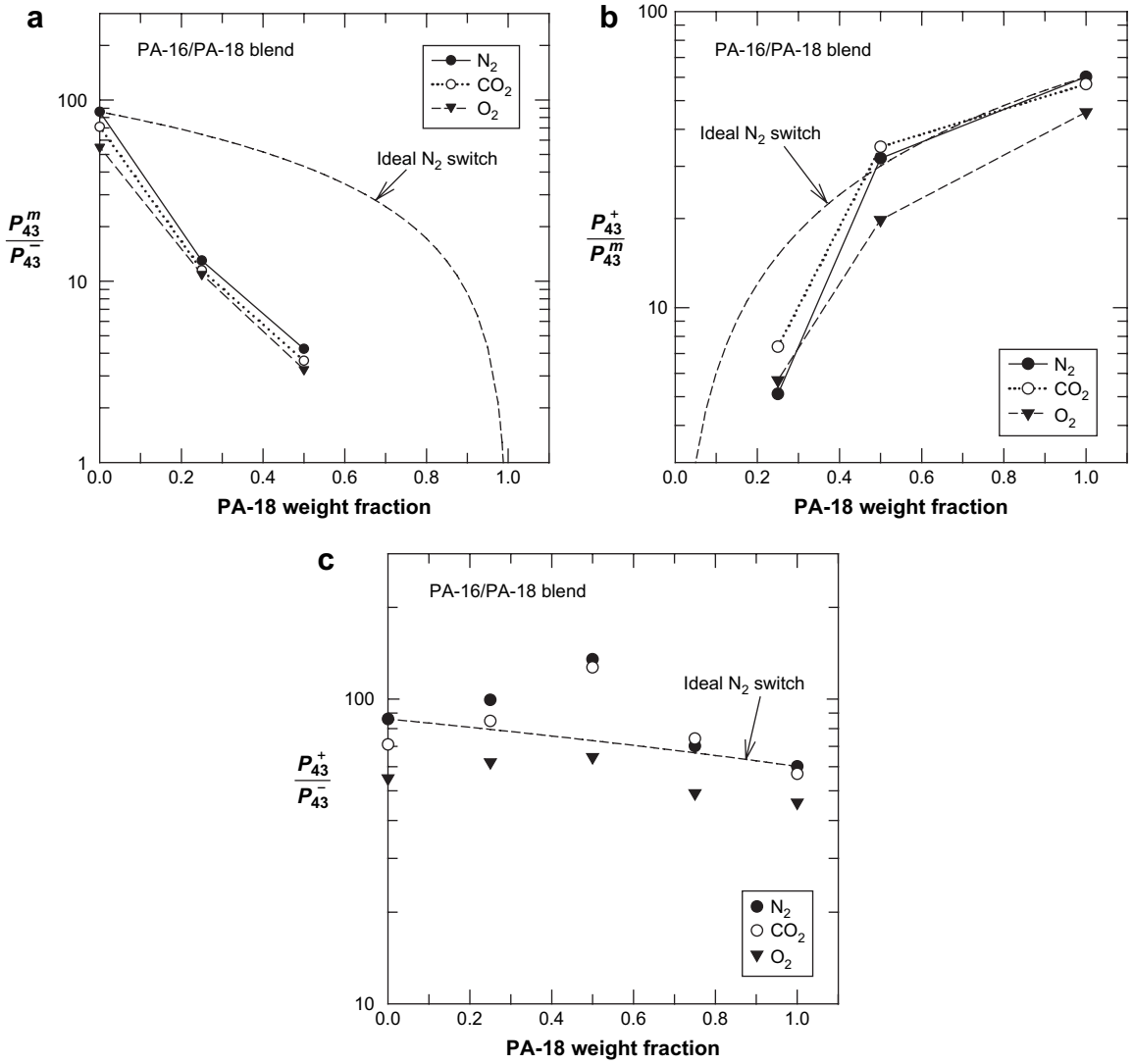

Fig. 12. The magnitude of O_2, N_2, and CO_2 permeation jumps for PA-16/PA-18 blends as a function of composition for (a) the PA-16 component, (b) the PA-18 component, and (c) the overall blend. Note: the baseline for the PA-16(25 wt%)/PA-18(75 wt%) blend was assumed to be well established when computing the magnitude of the overall permeation jump.

the overall permeation switch for PA-16(25)/PA-18(75) was calculated assuming the data provides an adequate permeation baseline for extrapolation. The maximum seen for the overall blend permeation jump at 50/50 weight blend is consistent with trends seen among the homologous series of *n*-alkyl acrylate polymers as shown in Fig. 13. As the side-chain length increases so does the crystallinity and the molten state free volume, both of which increase the jump magnitude. Blending PA-16 and PA-18 leads to an increase in the thermal switch beyond that achievable by the pure homopolymers apparently due to changes in the crystal morphology. Further understanding of the crystalline morphology may help to optimize the magnitude of the thermal switch effect.

4.3.3. Poly(tetradecyl acrylate) and poly(hexadecyl acrylate) blends

Fig. 14 shows the permeation responses for PA-14/PA-16 blends. There are two distinct endothermic peaks that are closely situated resulting in more overlap than the blend systems discussed earlier. Unlike previous cases, the O_2 permeation responses for the PA-14/PA-16 blends do not show a distinct permeation jump for the lower melting PA-14 component regardless of the blend composition, but rather a higher slope in this temperature range, presumably due to progressive melting, than might be expected by a simple Arrhenius response for a material of fixed morphology. A more familiar permeation jump occurs at the T_m of the higher melting component. In Fig. 14(b) the dashed line in the lower melting region defines an effective activation energy for O_2 permeation over the temperature range shown; the temperature range chosen for construction of such a line affects the value of the activation energy obtained. Similar lines were constructed for a few other blends and the effective activation energies obtained are shown in Table 2. Activation energies for permeation in homopolymers with $n = 14$, 16, and 18 obtained well below their T_m, i.e., no progressive melting, are shown

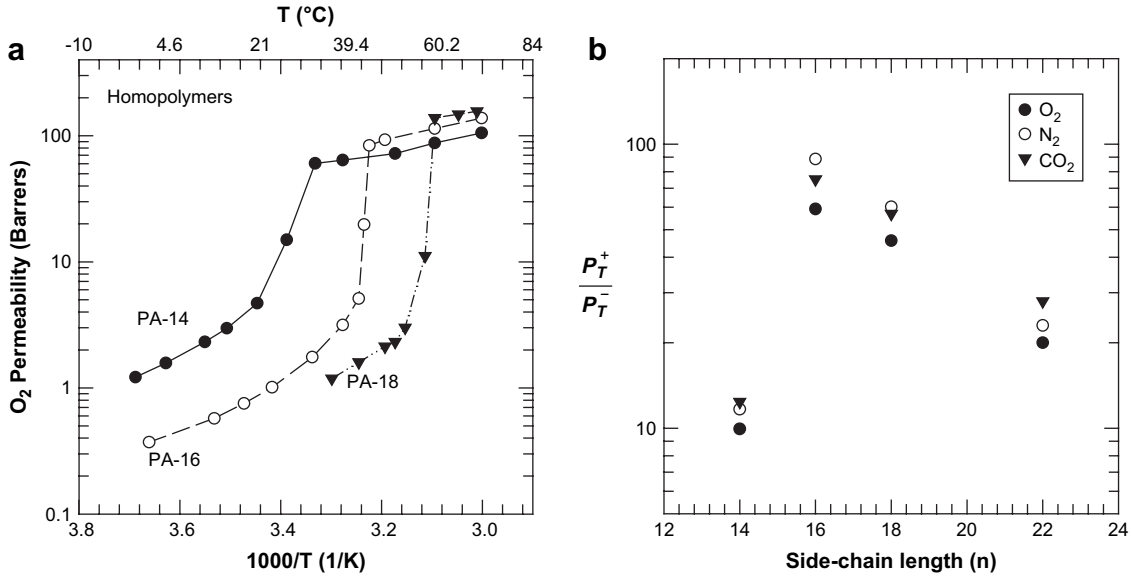

Fig. 13. (a) O_2 permeability of PA-14, PA-16, and PA-18 homopolymers as a function of temperature and (b) the magnitude of the O_2, N_2, and CO_2 permeation jumps for various homopolymers as a function of side-chain length where PA-22 from Ref. [25].

for comparison. When the side-chain lengths of the blend components are similar, the effective activation energies are considerably higher than for the homopolymers reflecting the nature of interaction of the two melting processes. The PA-14/PA-16 blends having the largest slopes or effective activation energies of the blends considered; significantly, this enhanced thermal response is in the temperature range of greatest interest, 0–30 °C, for produce distribution. The effect of temperature on the respiration rate of produce can also be represented by an Arrhenius relation; the activation energies for respiration of selected produce are shown in Table 3. The effective activation energies for the PA-14/PA-16 blends are more similar to that of some of the produce than the homopolymers listed in Table 2 or other potential membrane materials. Thus, the PA-14/PA-16 blends are promising candidates for more thermally responsive membranes for matching rates with produce over a range of temperatures.

As seen by the combined data for O_2 in Fig. 15, the value of the permeability coefficients of PA-14/PA-16 blends in the solid and molten states appears to be similar to the longer side-chain length component with differing activation energies. Since there is no well-defined intermediate state in these blends, the magnitude of the permeation jumps for the individual components could not be evaluated. Fig. 16 shows the overall permeation jump for the blend evaluated at 30 °C as a function of blend composition where there is a more or less additive relationship observed, except for N_2 and CO_2 which are slightly higher than additivity.

4.3.4. Ternary blends

Based on the above, a multi-component blend might be a simple route to emulate the response suggested in Fig. 1 for a multi-component laminate. To explore this possibility, the permeation response of a ternary blend of equal parts by weight of PA-14, PA-16, and PA-18 is shown in Fig. 17. The DSC scan shows resolvable melting points for the individual components; however, there are no distinct permeation jumps at the melting temperatures of the shorter side-chain length components. There is a single permeation jump close to the melting point of the longer side-chain component, PA-18. The magnitude of the permeation switch at 35 °C for the PA-18 component in the ternary blend was determined by assuming the intermediate state baseline starts just below the transition range of PA-18. Table 4 lists these values along with the ideal values for the magnitude of the permeation jump for a blend containing 33 wt% of PA-18 using an expression like Eq. (8). The magnitudes of the permeation jump for O_2 and N_2 are very similar to the ideal value; however, the magnitude of the switch for CO_2 is significantly higher than this ideal. Over the temperature region of 14–44 °C, the permeation response to temperature is nearly linear on the Arrhenius coordinates with an effective activation energy for O_2 and CO_2 permeation of 10.0 and 8.3 kcal/mol, respectively. Despite these values comparing well with that of homopolymers, listed in Table 2, the existence of closely melting components broadens the temperature range over which a more continuous permeation response is observed. The permeation response of the shorter side-chain length components in the ternary blend is somewhat hindered by the presence of the other component, similar to the PA-14/PA-18 and PA-16/PA-18 binary blends with lower concentrations of these components. To achieve greater temperature responsiveness for the ternary blend in the region of the lower melting components (i.e., temperatures reached during produce distribution) higher concentrations of these components than ideality would suggest are necessary. These results suggest that blends of several side-chain crystalline polymers might be a useful avenue for tailoring the temperature response of gas permeation.

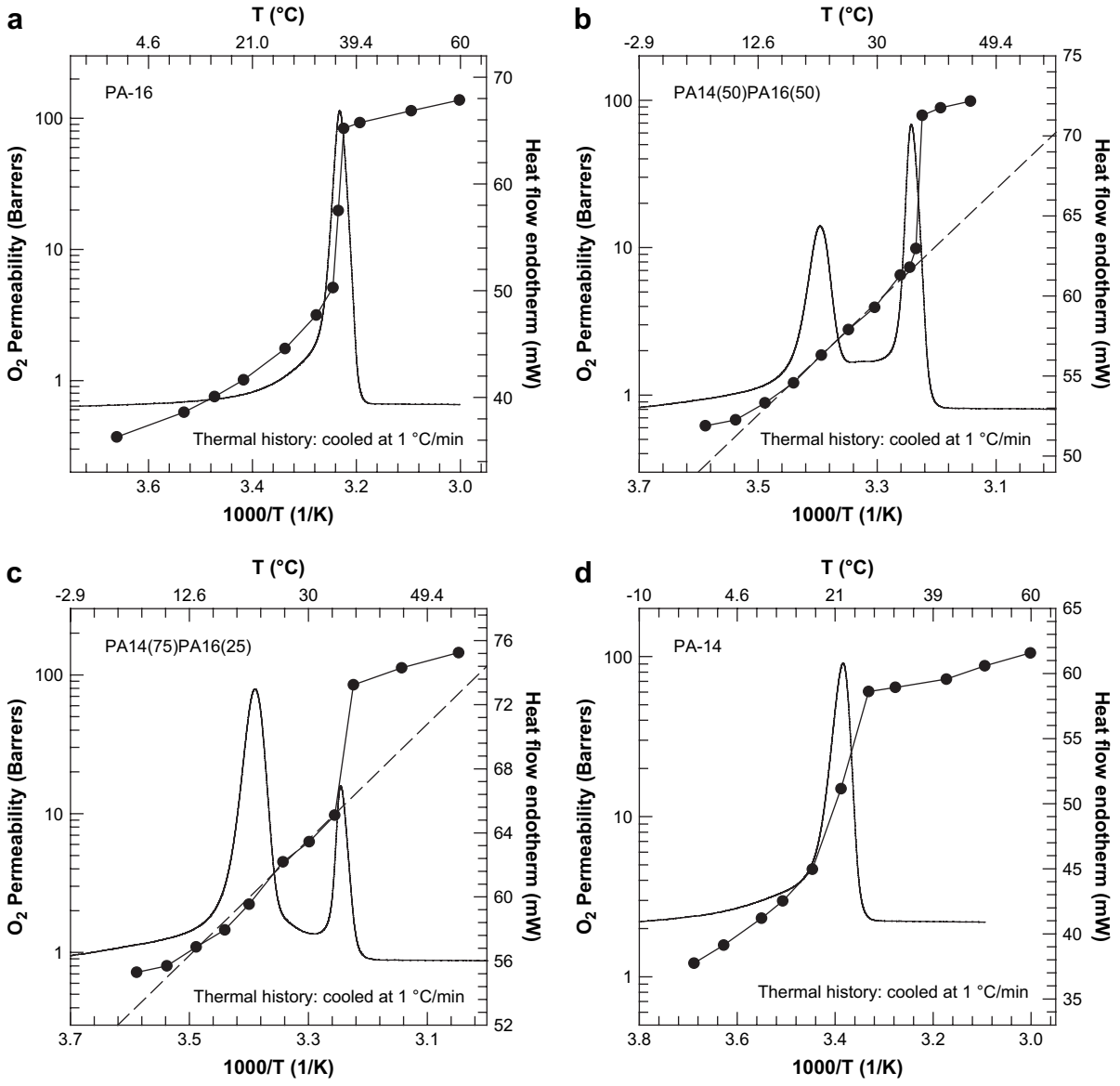

Fig. 14. O_2 permeability and DSC thermograms for (a) PA-16 homopolymer, (b) PA-14(50 wt%)/PA-16(50 wt%) blend, (c) PA-14(75 wt%)/PA-16(25 wt%) blend, and (d) PA-14 homopolymer.

4.3.5. Effect of blend composition on gas permeation

The literature [35–39] suggests that the permeability of gases in random copolymers and miscible blends should follow a simple relationship of the form:

$$\ln \boldsymbol{P} = \phi_1 \ln P_1 + \phi_2 \ln P_2 \tag{10}$$

in certain limiting cases. Here $\boldsymbol{P}_i$ and ϕ_i refer to the permeability and volume fraction of i in the homogeneous blend or copolymers. Deviations from this additive relationship have been documented: negative deviations in strongly interacting systems, positive deviations when P_1 and P_2 are very different,

Table 2
Comparison of activation energy for gas permeation, E_p (kcal/mol), of homopolymers and effective activation energies of blends

Polymer	E_{p,O_2}	E_{p,CO_2}	Temperature range (°C)
PA-14	8.5	7.6	2–12
PA-16	9.4	8.3	2–20
PA-18	11.0	10.3	30–40
PA-14(45)/PA-18(55)	12.0	11.3	5–45
PA-16(50)/PA-18(50)	13.6	12.5	5–45
PA-14(50)/PA-16(50)	15.2	14.7	5–35
PA-14(75)/PA-16(25)	16.5	16.6	5–35

Table 3
Comparison of activation energy for respiration, E_R (kcal/mol), of selected produce [40–43]

Produce	E_{R,O_2}	E_{R,CO_2}
Blueberry	35.2	39.0
Broccoli	15.0	15.8
Banana	11.3	9.8
Raspberry	10.7	13.3

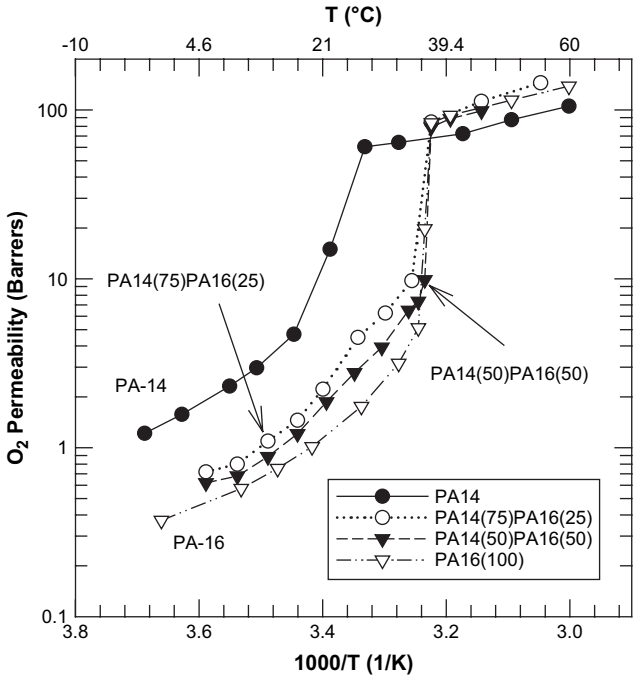

Fig. 15. O_2 permeability for PA-14/PA-16 blends as a function of temperature.

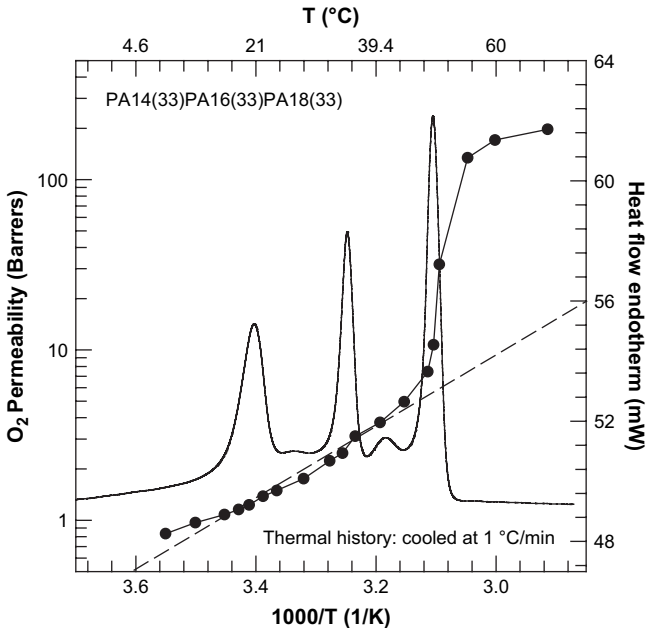

Fig. 17. O_2 permeability and DSC thermogram for a ternary blend containing equal parts by weight of PA-14, PA-16, and PA-18 as a function of temperature.

and S-shaped curves indicate at phase inversion in immiscible blend systems.

Fig. 18 shows the O_2 permeation–composition plots for blends at various temperatures. Below the melting point of the shorter side-chain component and at a temperature in the intermediate state, the permeability for the blends lies well below or along the additive line. Crystallinity complicates this analysis; therefore, examining this relationship at or above the melting point for the blend components is more informative. Above the melting point of both components, the permeability for the PA-14/PA-18 blends and PA-16/PA-18 blends shows more or less additivity of the pure component permeability coefficients. The PA-14/PA-16 blends have permeability values that are closer to that of the longer side-chain length component and, therefore, show a positive deviation from the additive line.

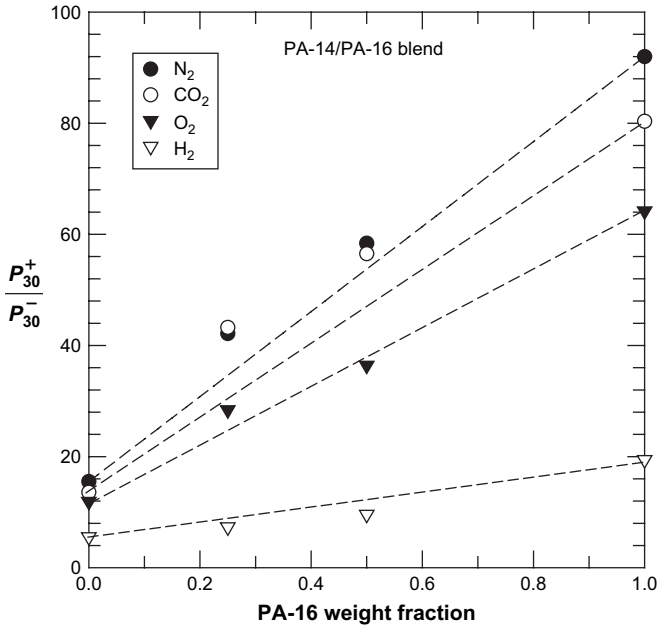

Fig. 16. The magnitude of N_2, CO_2, O_2, and H_2 permeation jumps for PA-14/PA-16 blends as a function of composition.

4.3.6. Effects of thermal history on semi-crystalline blends

Changes in crystalline morphology due to differences in thermal history have a significant effect on permeation, thermal and structural properties of poly(*n*-alkyl acrylate) homopolymers [9,26]. For homopolymers, Mogri and Paul found that slow cooled films lead to higher permeability in spite of having a higher crystallinity [25]. It is clear that simple crystallinity considerations are insufficient to fully explain this phenomenon and that a better understanding of crystallite size, shape, and orientation is necessary. As might be expected, the same trends are observed for blends. Fig. 19 shows the permeation response for a homopolymer, PA-18, and a blend, PA-16(50)/PA-18(50), with the corresponding DSC thermograms in the lower panels for film samples formed by cooling rates of 0.1 and 1.0 °C/min from the melt state. As expected the melting points and crystallinity (i.e., heat of fusion) are higher for the slower cooled samples as more stable

Table 4
Magnitude of the permeation jump for the PA-18 component, (P_{35}^+/P_{35}^m), in the ternary blend and the ideal calculated for 33 wt% PA-18

Gas	Ternary $(P_{35}^+/P_{35}^m)_{PA\text{-}18}$	Ideal $w_{PA\text{-}18}(P_{35}^+/P_{35}^m)^o_{PA\text{-}18}$
O_2	18.3	21.5
N_2	36.7	42.3
CO_2	56.0	29.5

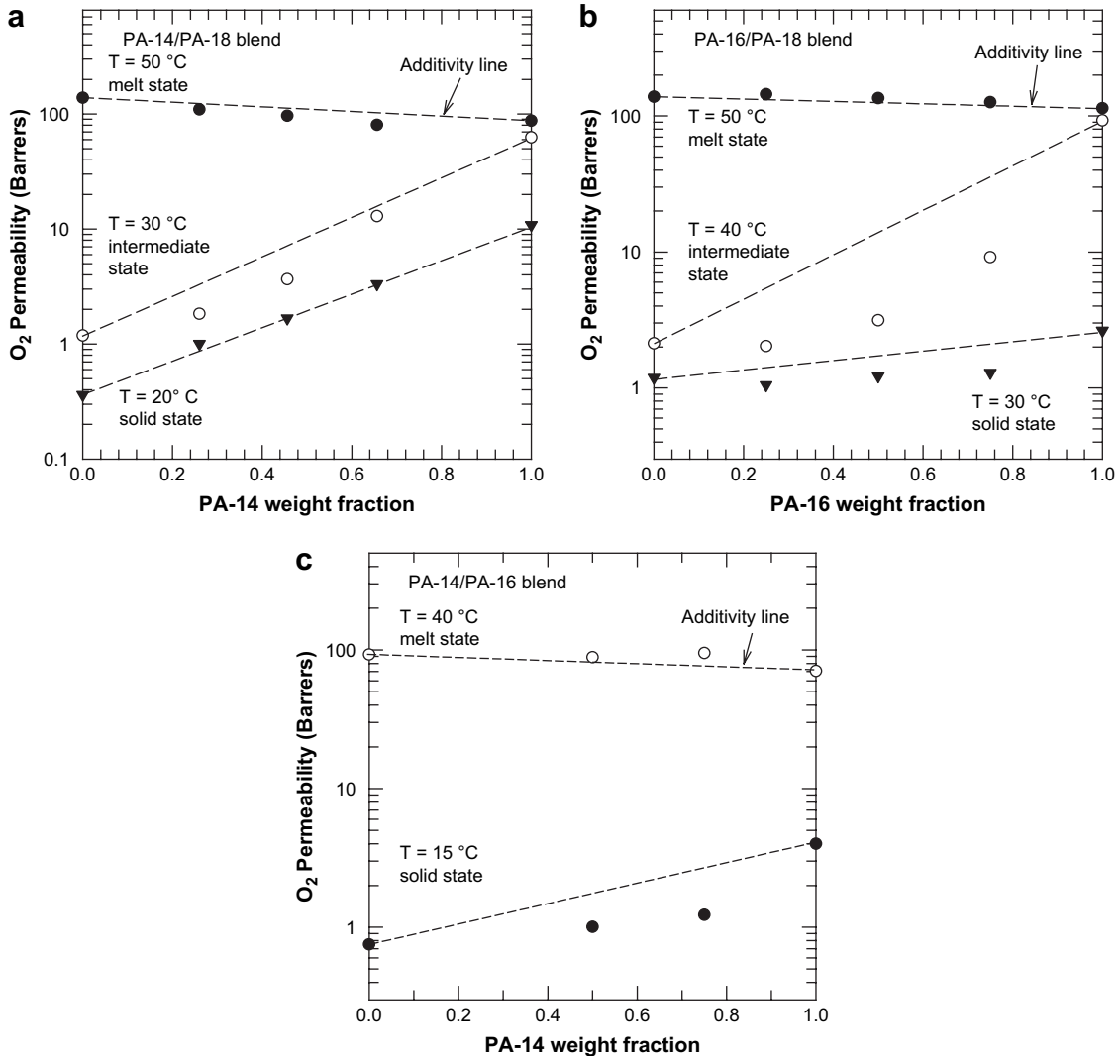

Fig. 18. O_2 permeability for (a) PA-14/PA-18, (b) PA-16/PA-18, and (c) PA-14/PA-16 blends as a function of composition in various states, solid state ($T < T_{m1} < T_{m2}$), intermediate state ($T_{m2} > T > T_{m1}$), and melt state ($T \geq T_{m2} > T_{m1}$).

crystals are formed. The more rapidly cooled films for PA-18 and PA-16(50)/PA-18(50) blend samples have lower permeabilities. As the temperature increases to the intermediate state, the difference between the permeability coefficients of the two cooling rates narrows. The activation energy of permeation for the slow cooled samples is lower than that of the 1.0 °C/min cooled samples. Table 5 summarizes the E_p values for each of the samples with the two thermal histories; E_p is always lower for the slower cooled samples of the homopolymer and the blend. For the blend in the intermediate state, there is a smaller difference between E_p for the two cooling rates suggesting that the barrier to permeation has been reduced by the melting of PA-16 crystallites.

Table 5
Effects of thermal history on the activation energies, E_p (kcal/mol), of O_2, N_2, and CO_2 permeation for PA-18 and PA16(50)/PA18(50) samples

Polymer	Sample state	Cooling rate (°C/min)	E_{p,O_2}	E_{p,N_2}	E_{p,CO_2}
PA-18	Solid	0.1	8.0	9.5	7.0
		1.0	9.4	9.3	9.1
PA-16(50)/PA-18(50)	Solid	0.1	8.8	10.7	8.0
		1.0	9.7	16.0	12.8
PA-16(50)/PA-18(50)	Intermediate	0.1	9.2	10.7	10.1
		1.0	11.1	13.3	12.3

5. Conclusions

The permeation response of semi-crystalline poly(*n*-alkyl acrylate) and poly(*m*-alkyl acrylate) blends as a function of temperature is significantly influenced by the side-chain lengths, *n* and *m*, of the blend components and blend composition. The components of each system crystallize independently of one another without any significant co-crystallization; however, the heat of fusion determined by various methods suggest that the presence of one component hinders crystallization of the other component. Changes in morphology by blending significantly influence the gas permeability as the melting temperature is traversed. PA-14/PA-18 and PA-16/PA-18 blends show two distinct permeation jumps at the melting point of each component. The permeation

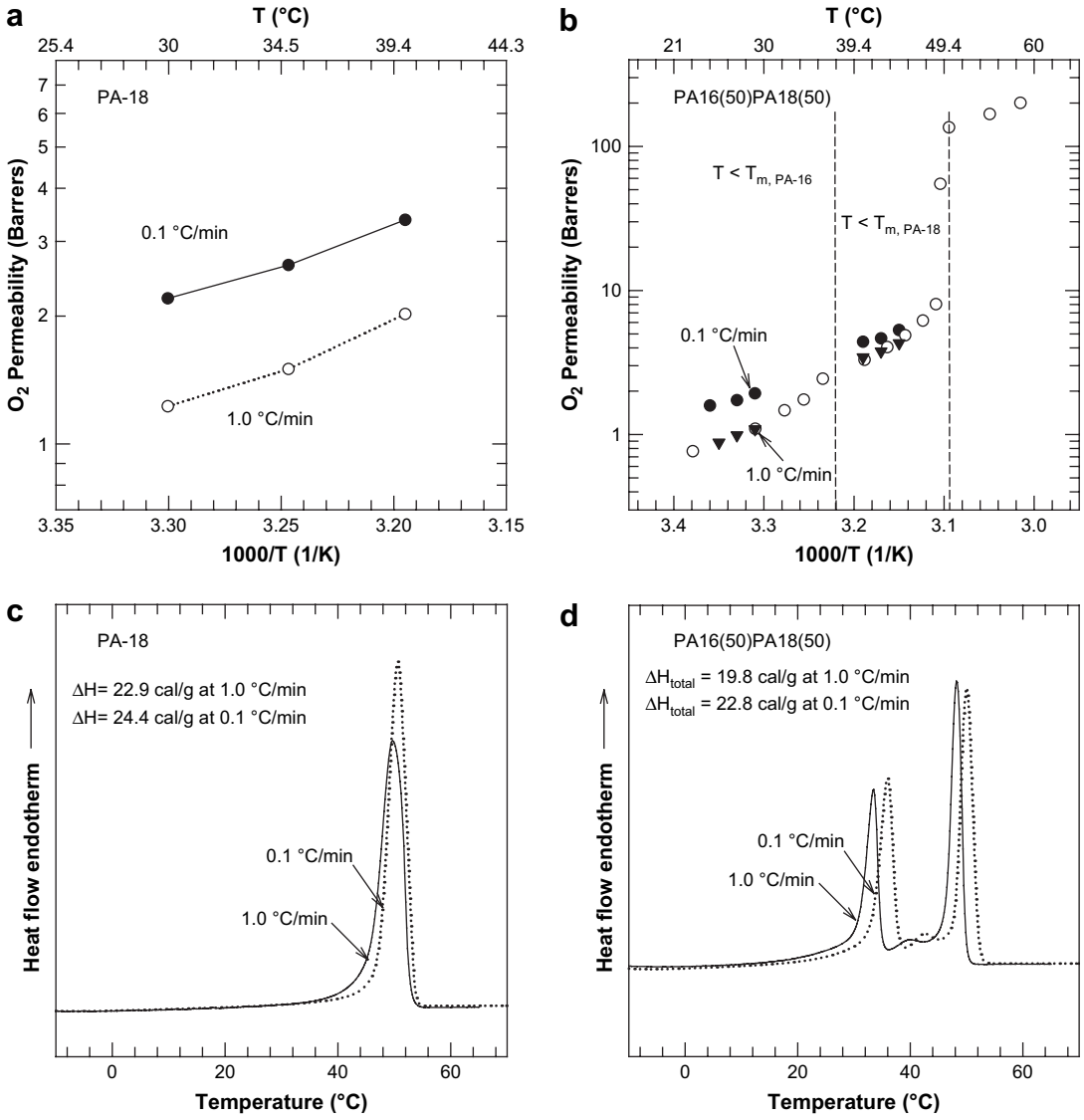

Fig. 19. Effects of thermal history on O_2 permeability of (a) PA-18 homopolymer and (b) PA-16(50 wt%)/PA-18(50 wt%) blend as a function of temperature at two cooling rates, 0.1 and 1.0 °C/min, with the corresponding DSC thermograms in the lower panels (c and d), respectively.

response of the PA-14/PA-16 and ternary blends did not show a jump at the melting point of PA-14 but showed a stronger temperature response, presumably due to progressive melting, than expected by simple Arrhenius considerations for such polymers where the crystalline morphology is fixed. This stronger temperature response occurs over the range of temperatures of interest for modified atmosphere packaging. This suggests that multi-component poly(*n*-alkyl acrylate) blends may be a route to obtain the necessary thermal responsiveness of gas permeation in membranes used in the packaging of respiring produce.

Acknowledgements

This material is based on work supported by the National Science Foundation under Grants CTS-0086961 and DMR-0423914.

References

[1] Rehberg CE, Fisher CH. Journal of the American Chemical Society 1944;66:1203–7.
[2] Greenberg SA, Alfrey T. Journal of the American Chemical Society 1954;76:6280–5.
[3] Kaufman HS, Sacher A, Alfrey T, Fankuchen I. Journal of the American Chemical Society 1948;70:3147.
[4] Wiley RH, Brauer GM. Journal of Polymer Science 1948;3:455–61.
[5] Overberger CG, Frazier C, Mandelman J, Smith HF. Journal of the American Chemical Society 1953;75:3326–30.
[6] Pittman AG, Ludwig BA. Journal of Polymer Science, Polymer Chemistry Edition 1969;7(11):3053–66.
[7] Yokota K, Hirabayashi T. Polymer Journal (Tokyo, Japan) 1986;18(2): 177–80.
[8] Hirabayashi T, Yokota K. Polymer Journal (Tokyo, Japan) 1987;19(9): 1115–9.
[9] Mogri Z, Paul DR. Polymer 2000;42(6):2531–42.
[10] Artyukhov AI, Borisova TI, Birshtein LL, Dmitrochenko DA, Shevelev VA. Vysokomolekulyarnye Soedineniya, Seriya A 1975; 17(11):2552–7.

[11] Crevoisier Gd, Fabre P, Corpart J-M, Leibler L. Science 1999; 285(5431):1246–9.
[12] Clarke R. Temperature switchable pressure sensitive adhesives. In: Adhesives age, vol. 36; 1993. p. 39.
[13] Temperature compensating films for produce. In: Prepared foods, vol. 161. Business News Publishing Co.; 1992. p. 95(91).
[14] Exama A, Arul J, Lencki RW, Lee LZ, Toupin C. Journal of Food Science 1993;58(6):1365–70.
[15] O'Leary KA, Paul DR. Polymer 2006;47(4):1226–44.
[16] O'Leary KA, Paul DR. Polymer 2006;47(4):1245–58.
[17] Jordan Jr EF, Feldeisen DW, Wrigley AN. Journal of Polymer Science, Polymer Chemistry Edition 1971;9(7):1835–52.
[18] Mogri Z. Gas transport properties of side-chain crystalline polymers, PhD dissertation. University of Texas at Austin; 2001.
[19] Platé NA, Shibaev VP. Comb-shaped polymers and liquid crystals. New York: Plenum Press; 1987.
[20] Hsieh HWS, Post B, Morawetz H. Journal of Polymer Science, Polymer Physics Edition 1976;14(7):1241–55.
[21] Shibaev VP, Petrukhin BS, Zubov YA, Plate NA, Kargin VA. Journal of Polymer Science, Polymer Chemistry Edition 1971;9(8):2291–8.
[22] Crank J. Diffusion in polymers; 1968.
[23] Michaels AS, Parker Jr RB. Journal of Polymer Science 1959;41:53–71.
[24] Michaels AS, Bixler HJ. Journal of Polymer Science 1961;50:413–39.
[25] Mogri Z, Paul DR. Polymer 2001;42(18):7765–80.
[26] Shibaev VP, Petrukhin BS, Zubov YA, Plate NA, Kargin VA. Vysokomolekulyarnye Soedineniya, Seriya A 1968;10(1):216–26.
[27] Armarego WLF, Chai CLL. Purification of laboratory chemicals. 5th ed. Amsterdam: Butterworth-Heinemann; 2003.
[28] Mogri Z, Paul DR. Journal of Membrane Science 2000;175(2):253–65.
[29] Mogri Z. Gas transport properties of side-chain crystalline polymers, Chemical engineering. Austin: University of Texas at Austin; 2001. 289 p.
[30] Kirkland BS. Chemical engineering. Austin: University of Texas at Austin; 2007.
[31] Koros WJ. Sorption and transport of gases in glassy polymers, Chemical engineering. Austin, Texas: University of Texas at Austin; 1977. p. 253.
[32] Flory PJ. Journal of Chemical Physics 1949;17:223–40.
[33] Hemminger WF, Sarge SM. Journal of Thermal Analysis 1991;37(7): 1455–77.
[34] Mogri Z, Paul DR. Journal of Polymer Science, Part B: Polymer Physics 2001;39(10):979–84.
[35] Shur YJ, Ranby B. Journal of Applied Polymer Science 1975;19(5): 1337–46.
[36] Shur YJ, Ranby B. Journal of Applied Polymer Science 1976;20(11): 3105–19.
[37] Shur YJ, Ranby B. Journal of Applied Polymer Science 1976;20(11): 3121–31.
[38] Shur YJ, Ranby B. Journal of Macromolecular Science, Physics 1977; B14(4):565–72.
[39] Ranby BG. Journal of Polymer Science, Polymer Symposia 1975;51: 89–104.
[40] Song Y, Kim HK, Yam KL. Journal of American Society for Horticultural Science 1992;117(6):925–9.
[41] Hagger PE, Lee DS, Yam KL. Journal of Food Process Engineering 1992;15:143–57.
[42] Maneerat C, Tongta A, Kanlayanarat S, Wongs-Aree C. A transient model to predict O_2 and CO_2 concentrations in modified-atmosphere packaging of banana at various temperatures. In: CA '97 proceedings: Seventh International Controlled Atmosphere Research Conference: July 13–18, 1997, vol. 5. University of California, Davis; 1997. p. 191–7.
[43] Joles DW, Cameron Arthur C, Shirazi Ahmad, Petracek Peter D, Beaudry Randolph M. Journal of the American Society for Horticultural Science 1994;119(3):540–5.